Roman Coronagraph Instrument Post Processing Report - OS11 HLC Distribution

January 7, 2025

Marie Ygouf[1], John Krist[1], Amelia Konomos[1], Kevin Zvonarek[1], Rob Zellem[2], Neil Zimmerman[2], Vanessa Bailey[1]

1. Jet Propulsion Laboratory, California Institute of Technology
2. Goddard Flight Space Center

Contents

1 Introduction

This document reports on findings from applying post-processing techniques to the Observation Scenario 11 - Hybrid Lyot Coronagraph simulated data for the Roman Space Telescope Coronagraph Instrument. This is an on-going work and thus the information contained in this document is subject to future updates. In the meantime, please send questions and/or comments to marie.ygouf@jpl.nasa.gov.

1.1 Key Definitions

CGI: Coronagraphic Instrument
EMCCD: Electron Multiplying Charge Coupled Device
GSFC: Goddard Space Flight Center
HLC: Hybrid Lyot Coronagraph
JPL: Jet Propulsion Laboratory
MUFs: Model Uncertainty Factors
OS: Observing Scenario
STOP: Structural Thermal Optical Performance
WFI: Wide Field Instrument

2 Data Description

2.1 OS11 Simulation

The Observing Scenario (OS) image time sequences are generated by John Krist and the integrated modeling team at JPL to create simulated CGI data for the Hybrid Lyot Coronagraph (HLC) which includes the most updated concept of operations observing strategy. For this work, we used the most recent OS dataset made public on July 11th 2023 (version 3), called OS11[1], with the broadband HLC 20190210 (Phase B flight design) in a 10% bandpass filter centered at 575 nm (Band 1: 546 - 603 nm). These HLC simulations are intended for evaluating post-processing algorithms. OS11 is representative of a realistic observing sequence, but does not reflect any particular requirements for total observation time, number of rolls, etc. (there is a limit of about $\pm 13°$ on maximum roll relative to the nominal solar normal orientation). OS11 is expected to be the last end-to-end time series. The target star used for these simulations is 47 UMa (V=5.0 mag, G1V, D_{star}=0.9 mas) and the reference star is ζ Pup (V=2.25 mag, O4I, D_{star}=0.4 mas). This reference star was chosen to keep solar pitch change to 3.5° to avoid large thermal changes. The stellar spectra of the two stars (G1V and O4I), and stellar diameter are included.

The observing sequence begins with a slew from a Wide Field Instrument (WFI) high latitude survey target to the reference star, followed by an observatory settling time and dark hole restoration, assuming that the dark hole was previously dug at some earlier time. Then, the observation cycle starts with 3/4 hour imaging ζ Pup before slewing to the target

---

[1]

star 47 UMa. The target is observed for about 6 hours at rolls angles of -13°, +13°, -13°, +13° relative to the solar-normal roll before slewing back to ζ Pup for about 3/4 hour of imaging. This observation cycle is repeated 4 times, with time between the 2nd and 3rd for one iteration of dark hole maintenance. Figure 1 shows a visualization of the OS11 HLC observing time series is presented. Note that the data corresponding to the dark hole touchup at the beginning of the whole observing sequence and cycle between cycles 2 and 3 is not included in the OS11 distribution.

The STOP (finite element & optical ray trace) model was run with 15 min timesteps to produce aberration and alignment changes. Misalignment-induced pointing offsets were compensated by repointing the observatory during ray tracing to ensure the star is always perfectly centered on the FPM (this excludes pointing jitter, which is a separate thing). Results were interpolated to 1 min timesteps. The STOP model assumed instantaneous slews, but the jitter model included slew/roll times. The model also includes thermal effects from solar angles, heaters, CGI mechanism movements (PAMs) & electronics.

These simulations include static optical errors (measured OTA & TCA, stand-in for phase-retrieval-derived optical error map, polarization aberrations, bulk shear of CGI relative to instrument carrier), Z4-Z37 aberrations vs time due to surface deformations & misalignments, OTA & TCA optics shifts vs time, bulk X,Y, CGI shear vs time at IC-CGI interface, "known" DM misalignments, "unknown" DM misalignments, dead actuator on DM1, DM bias, gain errors over DMs, DM stroke quantization, CGI DM & Lyot stop offsets vs time from bench deformations & tilts at IC-CGI interface, DM surface change due to thermal variations and imperfect FPM (both known and unknown errors).

Those simulations were produced with optical model uncertainties (MUFs). The following optical MUFs are always included: structural deformation = 2.0× (increases beam shear, wavefront error drift by 2x) and frequency-dependent jitter = 3.0× (<20 Hz), 4.27× (40-100 Hz) and 8.0× (>100 Hz). The following optical MUFs are included only when specified: polarization aberrations = 1.5×, contrast sensitivity to low-order aberrations = 2.0× (includes sensitivity to polarization and wavefront jitter)

2.2 Differences with previous observing scenarios

The successive observing scenarios that have been simulated since OS1 take into account the evolution of telescope and instrument design as well as the most updated concept of operations observing strategy. This section covers the major differences between OS11 and OS9[2], for which a similar data processing and analysis was performed (Ygouf et al., 2021).

2.2.1 Observing strategy

Both observing scenarios follow the same pattern of two pairs of science target observations at each roll angle, encapsulated by observations of the reference star.

The number of cycles is smaller for OS9 (3 cycles) than for OS11 (4 cycles). OS9 totals about 26 hours of observing time including about 20 hours on the target 47 UMa and about 6 hours on the reference ζ Pup while OS11 totals about 29 hours of observing time including about 26 hours on the target 47 UMa and about 3 hours on the reference ζ Pup.

Reference star images have batch ID's starting with 0 and incrementing by 1 with each visit
Target star images have batch ID's starting with 100 and incrementing by 1 every roll;
each cycle of target imaging starts at the next increment of 100

Cycle 1   Cycle 2   Cycle 3   Cycle 4

Batch ID= 0 100 101 102 103 1 200 201 202 203 2   3 300 301 302 303 4 400 401 402 403 5

Reference
Target (Cycle 1, Roll 1 = -13°)
Target (Cycle 1, Roll 2 = +13°)
Target (Cycle 1, Roll 3 = -13°)
Target (Cycle 1, Roll 4 = +13°)
Reference
Target (Cycle 2, Roll 1 = +13°)
Target (Cycle 2, Roll 2 = -13°)
Target (Cycle 2, Roll 3 = +13°)
Target (Cycle 2, Roll 4 = -13°)
Reference
EFC Probes
GITL
Reference
Target (Cycle 3, Roll 1 = -13°)
Target (Cycle 3, Roll 2 = +13°)
Target (Cycle 3, Roll 3 = -13°)
Target (Cycle 3, Roll 4 = +13°)
Reference
Target (Cycle 4, Roll 1 = +13°)
Target (Cycle 4, Roll 2 = -13°)
Target (Cycle 4, Roll 3 = +13°)
Target (Cycle 4, Roll 4 = -13°)
Reference

170   180   190   200   210

Hours

EFC Probes: apply pre-defined DM patterns & record resulting
image changes; no images are provided for this span
GITL: Download probe images to ground, use them to derive
wavefront error, compute new DM solutions, upload them
to CGI

Figure 1: Visualization of the observing sequence simulated in the OS11 HLC PSF time series. The sequence begins with a slew from a WFI high latitude survey followed by an observatory settling time and dark hole restoration. Then, Cycle 1 starts with 3/4 hours of imaging the reference ζ Pup before slewing to the target 47 UMa. The target is observed at two different roll angles before going back to the reference. This cycle is repeated 4 times in total. Data corresponding to the EFC maintenance at the beginning of Cycles 1 and 3 are not included in the OS11 distribution.

Another difference between OS9 and OS11 is the 4-hour Electric Field Conjugation (EFC) maintenance on ζ Pup performed before cycles 1 and 3 for OS11 while it is performed at the beginning of each cycle in OS9. Those EFC data are not included in the distribution.

Finally, while the reference star was observed in analog mode in OS9, it is now observed in photon-counting mode in OS11.

2.2.2 Astrophysical targets

The target, 47 UMa (V=5.0 mag, G1V, D_{star}=0.9 mas), has been used for all observing scenarios since OS1, including OS9. The reference star, ζ Pup (V=2.25 mag, O4I, D_{star}=0.4 mas) was used for the first time in OS9. Although being located 90 degrees away from 47 UMa, this reference star was selected because it is only 3.5 degrees different in solar pitch from 47 UMa. In the previous observing scenarios, β UMa and η UMa were both used. A higher-fidelity observatory model incorporated in OS8 simulations showed a greater sensitivity of the primary mirror wavefront to the solar pitch angle. This motivated switching the reference star to ζ Pup for OS9 for which the difference in solar pitch angle with 47 UMa is smaller (3.5 degrees instead of $\sim$ 15 degrees for previous reference stars). This reduced aberration drifts by over an order of magnitude. Most importantly, it reduced high-order spherical aberration drifts, which LOWFS cannot sense or control, to negligible levels.

2.2.3 Telescope and instrument modeling

The STOP model consists of nodes forming the mesh that represents the structure of the telescope and Coronagraph instrument (the wireframe representation of the system).

The OS9 STOP model did not have CGI, raytrace ended at FSM. The LOWFSC model was relatively simple and more optimistic. The OS11 STOP model includes CGI (including power and mechanisms), raytrace ended at FPM. A much more sophisticated LOWFSC model is included, but tuned for error budget instability levels, resulting in high-temporal frequency noise. The telescope model has also been updated for OS11.

A detector model was applied to the Roman Coronagraph images distributed with the public release of OS11 data with planets (hlc_os11_frames_with_planets.fits, hlc_os11_frames_with_planets_muf.fits). This detector model converts the noiseless speckle images to noisy images that would be obtained on the instrument EMCCD. In particular, speckle images were interpolated in time to produce images at EMCCD framerates (30 seconds and 27 seconds for target in the no-MUF and MUF cases respectively, 2 seconds and 2.2 seconds for reference in the no-MUF and MUF cases respectively), binned to the detector resolution (0.021 arcsec = 0.42 λ_c/D), and fed into the EMCCD model. Both target and reference stars are observed in "photon-counting" mode (see Section 3.1.4 for more details about this mode).

3 Data Reduction Procedure

3.1 Preparing data for post-processing

Before applying post-processing to the OS11 data, several steps are needed:

- Step 1: Create planet-free images;

- Step 2: Add detector noise to images;

- Step 3: Data extraction;

- Step 4: Apply photon-counting to noisy data and coadd noiseless data cubes;

- Step 5: Normalization to the flux incident on the illuminated area of the primary mirror.

It is worth noting that no cosmic rays or traps are included in the OS11 data sets. There is no need for procedures to correct those effects. Similarly, there is no need for dark subtraction or flat fielding. However, those effects will need to be corrected during the Roman Coronagraph operations.

3.1.1 Step 1: Create planet-free images

The OS11 distribution datasets include the time series speckle field images (without planets) without and with optical MUFs at CCD pixel sampling at 1 minute timesteps (hlc_os11_darkhole _noiseless.fits and hlc_os11_darkhole_muf_noiseless.fits) as well as temporal resampling of those time series with injected planets (hlc_os11_frames_with_planets.fits and hlc_os11_frames _with_planets_muf.fits). We followed the steps described in the OS11 distribution description to generate our own planet-free datasets to evaluate the post-processing performance:

- The hlc_os11_planet_*.fits images oversample the detector pixels by 5x and should be 5x5 binned down to match. The images are primary-normalized flux. Each image is [nx=275,ny=275] pixels;

- Multiply the binned image by planet/star contrast ratio and stellar flux, to convert to e-/sec flux units (pre-electron-amplification);

- Add the planet images to the target images from hlc_os11_darkhole_*.fits, matching appropriate orientations. Files hlc_os11_planet_r3.5_t-13_oversampled.fits, hlc_os11_planet _r3.5_t13_oversampled.fits, hlc_os11_planet_4.5_t117_oversampled.fits and hlc_os11_planet _r4.5_t143_oversampled.fits contains simulations of point sources offset from the star by 3.5 4.5 λ_c/D (176 226 mas) at angles of -13°, +13°, 117°, 143° (representing the two rolls) and with contrasts of 2e-9 @ 4.5 λ/D and 5e-9 @ 3.5 λ/D;

- Interpolate the images having the same batch ID over time to match the selected exposure frame time.

3.1.2 Step 2: Add detector noise to images

We used the script hlc_os11_example.py provided as part of the OS11 distribution to add detector noise to images. The script loops over all the frames from the time series speckle field images and adds detector noise as needed using the emccd_detect package.[3]

---

[3]emccd_detect is a Python package for EMCCD modeling provided by Bijan Nemati, Sam Miller, and Kevin Ludwick: https://github.com/wfirst-cgi/emccd_detect

Target	Batch ID #	Cube dimensions no MUFs	Cube dimensions MUFs
	0	$55 \times 55 \times 1147$	$55 \times 55 \times 1055$
	1	$55 \times 55 \times 991$	$55 \times 55 \times 911$
	2	$55 \times 55 \times 991$	$55 \times 55 \times 911$
ζ Pup	3	$55 \times 55 \times 1147$	$55 \times 55 \times 1055$
	4	$55 \times 55 \times 991$	$55 \times 55 \times 911$
	5	$55 \times 55 \times 991$	$55 \times 55 \times 911$
	101	$55 \times 55 \times 194$	$55 \times 55 \times 215$
	103	$55 \times 55 \times 194$	$55 \times 55 \times 215$
	200	$55 \times 55 \times 194$	$55 \times 55 \times 215$
47 UMa -13°	202	$55 \times 55 \times 194$	$55 \times 55 \times 215$
	301	$55 \times 55 \times 194$	$55 \times 55 \times 215$
	303	$55 \times 55 \times 194$	$55 \times 55 \times 215$
	400	$55 \times 55 \times 194$	$55 \times 55 \times 215$
	402	$55 \times 55 \times 194$	$55 \times 55 \times 215$
	100	$55 \times 55 \times 194$	$55 \times 55 \times 215$
	102	$55 \times 55 \times 194$	$55 \times 55 \times 215$
	201	$55 \times 55 \times 194$	$55 \times 55 \times 215$
47 UMa +13°	203	$55 \times 55 \times 194$	$55 \times 55 \times 215$
	300	$55 \times 55 \times 194$	$55 \times 55 \times 215$
	302	$55 \times 55 \times 194$	$55 \times 55 \times 215$
	401	$55 \times 55 \times 194$	$55 \times 55 \times 215$
	403	$55 \times 55 \times 194$	$55 \times 55 \times 215$

Table 1: Cubes dimensions for each batch ID / pointing.

3.1.3 Step 3: Data Extraction

We used the script hlc_os11_example.py provided as part of the OS11 distribution to extract frames from all batch IDs/pointings for the reference star, and for the target at rolls +13° and -13° for each of the four available datasets. Table 1 summarizes the dimensions for each of those cubes. It is worth noting that the total number of frames per batch ID may be different. Figure 2 shows the first frames of those data cubes for the noisy case without model uncertainty factor.

3.1.4 Step 4: Apply photon-counting to noisy data and coadd noiseless data cubes

Apply photon-counting to noisy data. The Roman Space Telescope Coronagraph uses an Electron-Multiplying CCD (EMCCD) as a detector. A high voltage gain register amplifies the signal before read noise is added, which reduces read noise in proportion. This reduction comes at the cost of an increase (by a factor of $\sim \sqrt{2}$), called as Excess Noise Factor (ENF) of all other noises. This latter disadvantage can be mitigated using a processing technique called photon counting. In photon counting, a high gain (1000 or more) is applied to each EMCCD frame. A threshold factor, typically a few times (5 is usually good) the read noise, is chosen. Any pixels with counts below the threshold are recorded as zero electrons, while

any above are recorded as one electron. No more than 1 electron will ever be recorded, regardless of how many input electrons generated the signal. The final image is the sum of separate photon-counted frames. The script hlc_os11_example.py is performing photon-counting on both target and reference stars using PhotonCount.[4] For more details about the photon-counting procedure, the reader can refer to Nemati et al. 2020 and Ygouf et al. 2021.

The following steps were performed for each frame of noisy data:

- Apply threshold to each frame of data cube. We chose a threshold factor of 5 (5 times read noise, note that read noise can be found in the FITS header) in this case. Binary images were obtained in output;

- Co-add frames in data cube along the temporal dimension;

- Correct for the coincidence and threshold losses;

- Background correction is performed by averaging a subset of 36 pixels in the corner of the image;

- Normalization by the frame exposure time to obtain an image in count/sec.

After this processing, each data cube of dimension 6×55×55 is composed of 6 averaged frames, one per pointing. Figure 3 shows the coadded frames after applying the photon counting processing for the noisy case without MUF.

Normalize and coadd noiseless data.   OS11 noiseless data are in average flux units, and they do not have photon quantization or an EMCCD model applied. Therefore, noiseless data cubes do not need to be photon-counted. However, two steps need to be performed to preprocess those data cubes:

- Co-add frames in data cube along the temporal dimension;

- Normalization by the frame exposure time to obtain an image in count/sec;

- Dividing by the gain in the case of noisy data for reference the star (note that the gain can be found in the FITS header).

The noiseless datacubes are converted to 6×55×55 data cubes, one for the reference, and one for the target at each roll, where each frame corresponds to the coadded frames for each batch ID or pointing.

---

[4]PhotonCount is a Python package for EMCCD photon-counting post-processing provided by Bijan Nemati, Sam Miller, and Kevin Ludwick: https://github.com/wfirst-cgi/PhotonCount

Star	MUFs	Exp. time/fr. (s)	Detector Mode	EM gain
47 UMa	No	30	Photon-counting	5000
ζ Pup	No	2	Photon-counting	5000
47 UMa	Yes	27	Photon-counting	5000
ζ Pup	Yes	2.2	Photon-counting	5000

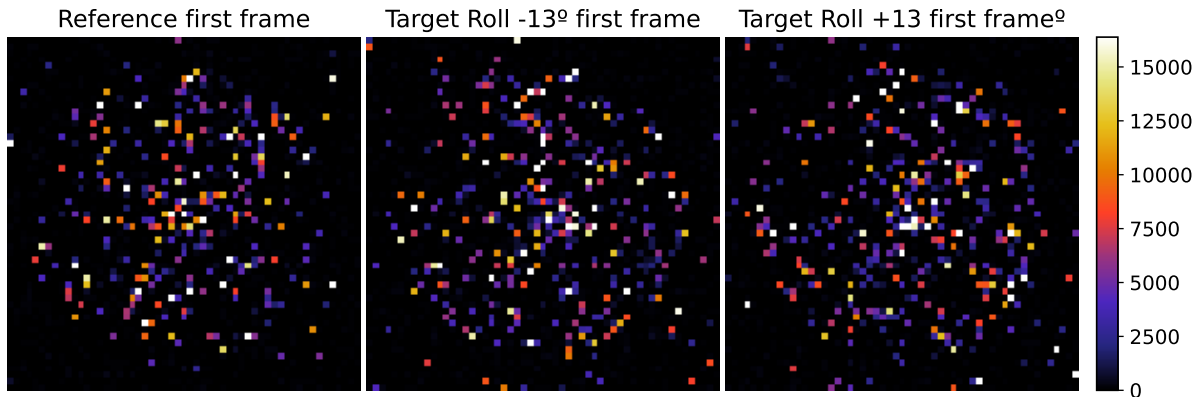Table 2: EMCCD setup for target and reference stars.

Figure 2: Raw EMCCD frames in photon-counting mode for the noisy case with planets and with MUFs.

3.1.5 Step 5: Normalization

At the end of step 4, the data units are count/sec. In step 5, we normalize the data to contrast units. In order to perform this step, we need to estimate the peak flux of the unocculted point spread function (PSF) at the detector sampling.

The OS11 distribution contains images of a flat-spectrum source offset by various amounts in radius and angle from the center of the FPM over one quadrant of the dark hole (hlc_os11 _psfs_oversampled.fits). It is a $[nx,ny,r,\theta] = [275,275,21,36]$ array. Those images are normalized to the flux incident on the illuminated area of the primary mirror (primary-flux-normalized). There are no losses from reflections, filters, QE, etc, but losses from CGI's masks are included in the simulation. In the absence of masks, the total image intensity would be 1.0. These 275×275 pixel images are sampled by 0.08 λ_c/D.

We first need to resample source offset images to the detector pixel size (0.435 λ_c/D) by binning them down to 55×55. Then we extract the maximum value from the entire datacube. We divide the pre-processed target and reference star datacubes by this value to obtain primary-flux-normalized data cubes. Finally, we divide those cubes by the flux of star to obtain the normalization in contrast units.

The results of applying those 5 steps to the OS11 distribution datasets (with or without noise and with and without MUFs) are shown in Figure 4.
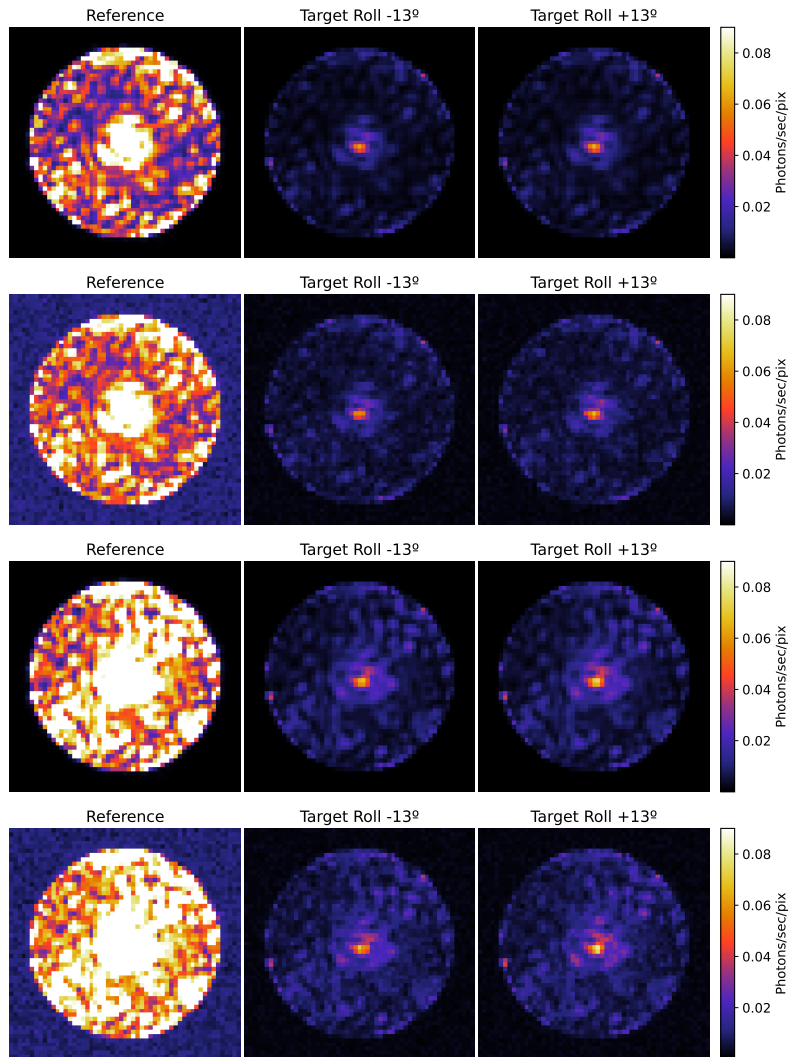
Figure 3: Gain corrected (reference) and photon-counted (target) data represented on the same color scale. From top to bottom: No MUF, Noiseless; No MUF, Noisy; MUF, Noiseless; MUF, Noisy.
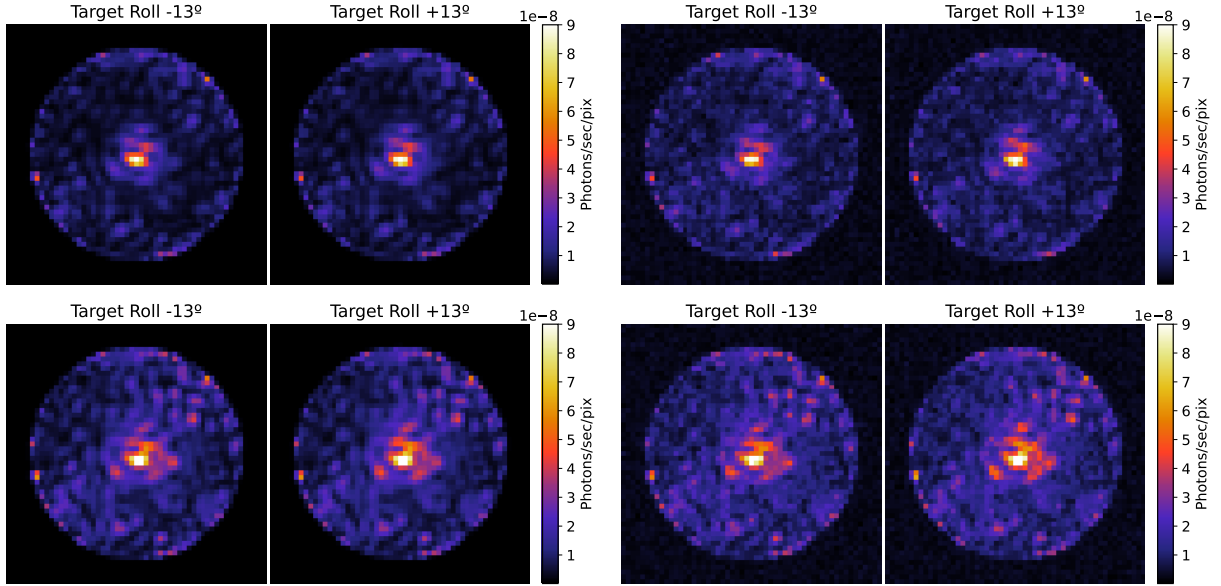
Figure 4: Pre-processed, coadded data for all datasets with planets in contrast units. [Top Left] No MUF, Noiseless. [Top Right] No MUF, Noisy. [Bottom Left] MUF, Noiseless, [Bottom Right] MUF, Noisy.

3.2 Post-processing

3.2.1 Procedure

We applied different techniques of post-processing, taking advantage of both the Reference Star Differential Imaging (RDI) and Angular Differential Imaging (ADI) strategies. RDI consists in observing a reference star to calibrate the stellar residuals. ADI consists in calibrating the stellar residuals by observing the target at different rolls angles (e.g., +/- 13 degrees).

Two families of techniques were explored:

- *Classical PSF subtraction.* Two flavors of this technique were implemented using either RDI or ADI, called cRDI and cADI respectively. Our implementation of classical PSF uses linear regressions to minimize the least square error in the final image (Figures 5 & 6);

- *Principal Component Analysis (PCA).* We used KLIP (Soummer et al. 2012), a Principal Component Analysis (PCA) technique that uses the reference cube as a library of reference point spread functions (Figure 7).

For the target at both rolls, each of the batch IDs (6 visits, 2 rolls each) was processed separately and combined at the end of the processing. We applied an annular mask, only taking into account the pixels that are comprised between 2.2 and 6 λ/D for both the regression and principal component analysis. The reason for this choice is that this region is the one we are the most interested in (the separations of the injected planets are $3.5\lambda/D$ and
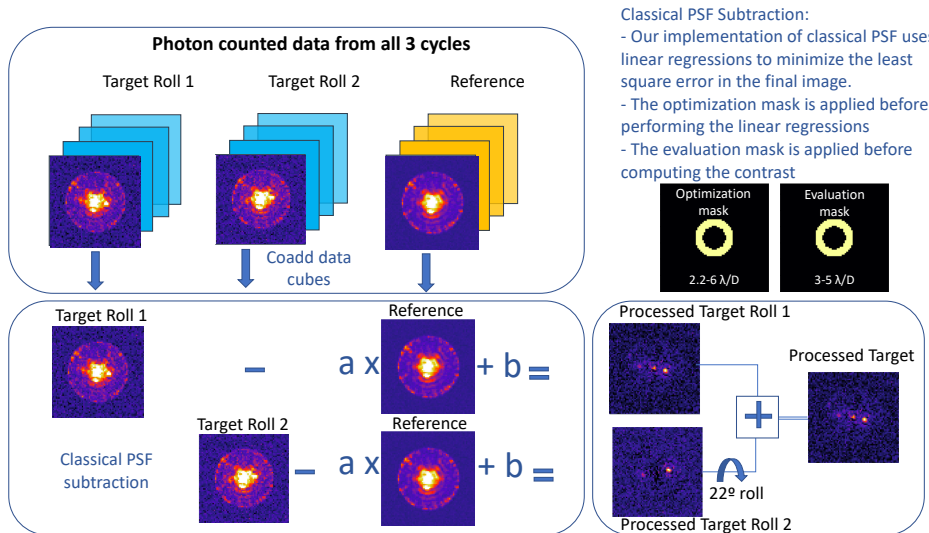
Figure 5: Performing Classical RDI (cRDI) PSF subtraction on OS11 HLC.

$4.5\lambda/D$ respectively) and using data outside of this region for post-processing may negatively impact the gain in this region.

Then, for RDI, we derotated the processed roll at $+13^{\underline{o}}$ and coadded with the processed roll at $-13^{\underline{o}}$. Figure 5 represents our data processing using RDI.

For ADI we did the same thing using the $-13°$ roll as a reference for the $+13°$ roll and using the $+13°$ roll as reference for the $-13°$ roll. We then derotated the processed $+13°$ roll that we coadded with the processed $-13°$ roll as we did before for RDI. Figure 6 represents our data processing using ADI.

We performed those processing for our 4 different data sets: with or without noise and with and without model uncertainty factor.

3.2.2 Results

Figure 8 shows the results of this processing for the processed cRDI, cADI and KLIP RDI data. Both planets at 2×10^{-9} and 5×10^{-9} are visible in the processed data for all 4 cases, being less visible in the noisy case where the noise is dominating over the speckles.

We computed contrasts and gains in an annular region including both planets, between 3 and 5 λ/D. To calculate the contrast, we computed the standard deviation per pixel in the region of interest given by the annular mask for each of the 6 visits and we computed the median of those 6 visits. For KLIP reductions, we compensated for over-subtraction from algorithmic throughput using forward modeling. This technique consists in implementing the same processing applied on the images on sources offset by various amounts in radius
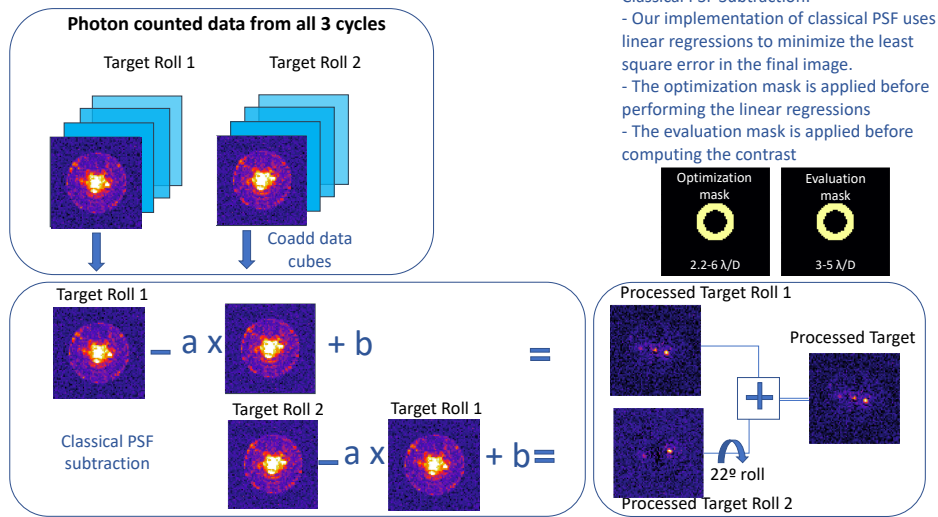
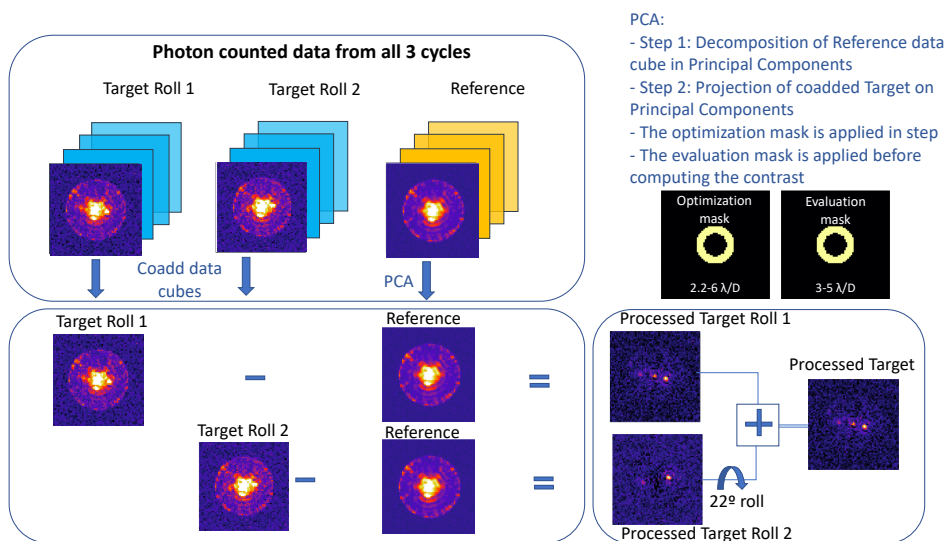Figure 6: Performing Classical ADI (cADI) PSF subtraction on OS11 HLC.

Figure 7: Performing KLIP RDI PSF subtraction on OS11 HLC.

from the center of the FPM, to estimate and correct for the impact of the post-processing algorithm on the planet throughput. Those computations were done on the data sets without planets to avoid any contamination from the planet signal. Note that the planets would need to be masked out if we were performing those computations on the data with planets.

The 5σ contrasts for the post-processed noiseless and noisy data are all below 3.6×10^{-9} and 1.3×10^{-8}, respectively, the noisy case with MUF being the worse case scenario. These values meet, with margin, the design requirement of 2.5×10^{-8} on the noisy data and the Threshold Technical Requirements 1×10^{-7}. In the noisy case, the noise is the limiting factor, which explains the observed difference in sensitivities up to 1 magnitude between the noiseless and the noisy cases.

The corresponding gains with respect to the unprocessed roll combined data vary significantly depending on if there is noise or not, the best gains (>4) being observed for the noiseless case. In the noisy case those gains decrease down to 1.3 when using classical ADI. When comparing the performance of RDI vs ADI, the best gain is observed with ADI in the case of noiseless data. Indeed ADI usually provides more stable wavefront errors, which is important for classical PSF subtraction. On the other hand, RDI performs better in the presence of noise. The higher shot noise from the science target speckles (versus the brighter reference star speckles) explains most of the difference in ADI performance as shown in Zimmerman et al.

We computed the Factor Above Classical (FAC), also called post-processing factor (fpp) in other documents, which is defined as the improvement in sensitivity over that achieved with classical RDI (or cRDI) PSF subtraction with a single observatory roll angle. This factor is defined for the noiseless case, because it is used in the Roman Coronagraph project error budget as an assumed attenuation factor on the speckles only. The factor above classical is computed with respect to the single roll processed with classical subtraction. The post-processing factor is equal to 1.9 and 1.7 for the KLIP RDI roll combined processing without and with MUFs respectively, which is the expected order of magnitude for those scenarios and in family with the results obtained from processing the OS9 distribution datasets (2 and 1.7 respectively). As a reference, we also computed the equivalent of those factors in the noisy cases without and with MUFs, which are equal to 1.5 and 1.4, which is well below 2. This is due to the fact that we are dominated by the detector noise in this case and KLIP does not add much improvement with respect to the classical subtraction technique in that regard. Tables 3 and 4 summarize the sensitivities, gains and FAC for the OS11 and OS9 data sets.

We compiled the same results in an annular between 6 and $9\lambda/D$, consistent with the TTR5 requirement. We observe better gains from classical RDI, ADI and KLIP RDI but worse FAC, the classical PSF subtraction performing significantly better on the 6 to $9\lambda/D$ annular mask than on the 3 and $5\lambda/D$ annular mask, which is closer to the star. This points to more stable speckles at large separations, which is to be expected. Table 5 summarizes the sensitivities, gains and FAC for the OS11 data set on the 6 to $9\lambda/D$ annular mask.
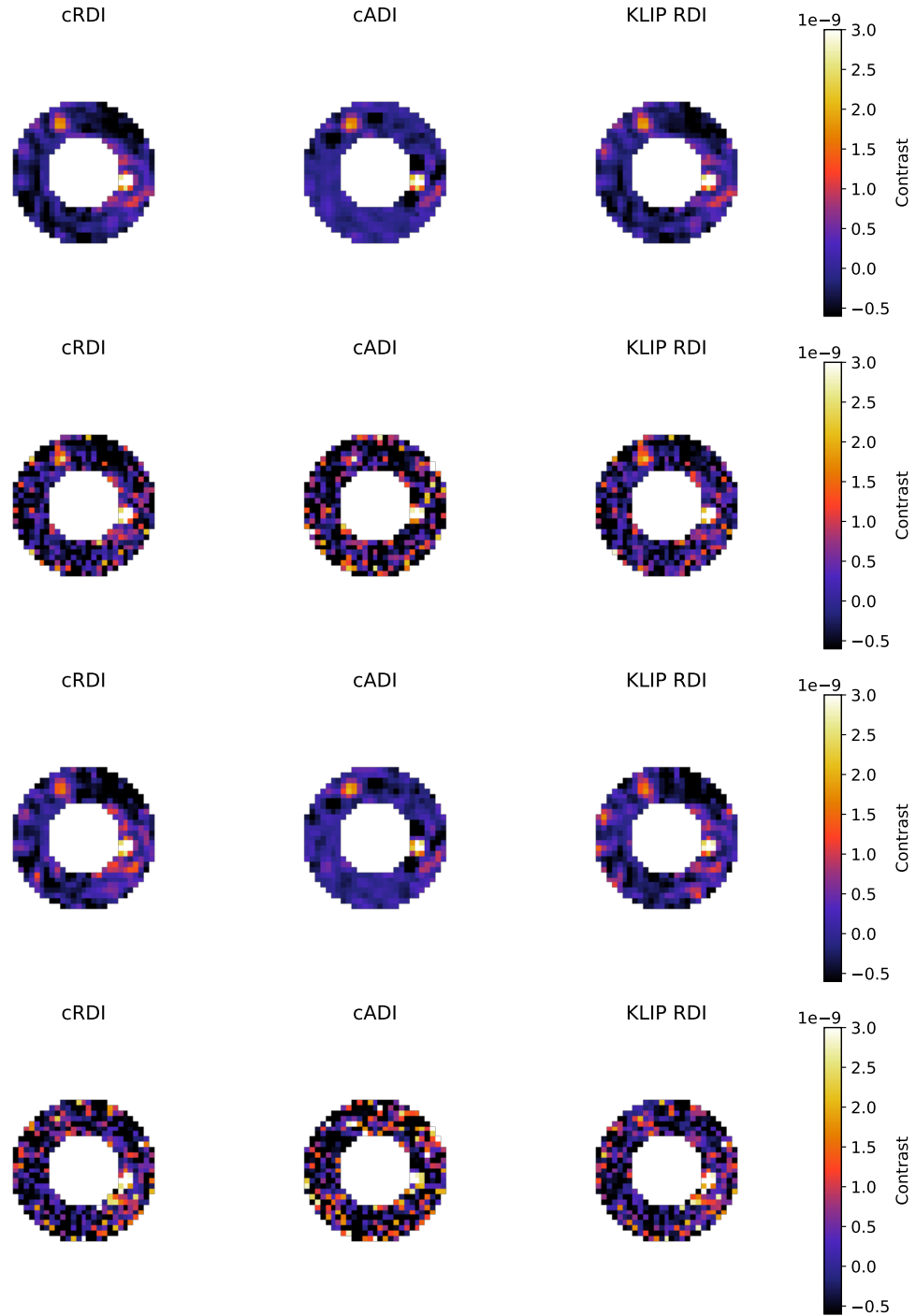
13

Figure 8: Datasets with planets processed with the 3 to $5\lambda/D$ annular mask with cRDI, cADI and KLIP ADI in contrast units. From top to bottom: No MUF, Noiseless; No MUF, Noisy; MUF, Noiseless; MUF, Noisy.

Post-Processing Method	Noiseless			Noisy		
	5σ contrast	Gain	FAC	5σ contrast	Gain	FAC
No MUFs						
No sub., single roll minus	1.0×10^{-8}			1.3×10^{-8}		
No sub., single roll plus	1.0×10^{-8}			1.3×10^{-8}		
No sub., roll combined	8.0×10^{-9}			9.6×10^{-9}		
cRDI, single roll	2.2×10^{-9}	4.7		8.7×10^{-9}	1.5	
cRDI, roll combined	1.5×10^{-9}	5.3	1.2	6.1×10^{-9}	1.6	1.1
cADI, roll combined	6.2×10^{-10}	12.8	2.6	7.7×10^{-9}	1.3	0.9
KLIP RDI, roll combined	1.2×10^{-9}	8.3	**1.7**	5.9×10^{-9}	2.0	1.4
With MUFs						
No sub., single roll minus	2.7×10^{-8}			2.9×10^{-8}		
No sub., single roll plus	2.7×10^{-8}			3.0×10^{-8}		
No sub., roll combined	2.1×10^{-8}			2.2×10^{-8}		
cRDI, single roll	3.6×10^{-9}	7.4		1.3×10^{-8}	2.3	
cRDI, roll combined	2.5×10^{-9}	8.4	1.1	8.5×10^{-9}	2.6	1.1
cADI, roll combined	1.1×10^{-9}	18.8	2.5	1.1×10^{-8}	2.0	0.9
KLIP RDI, roll combined	1.9×10^{-9}	14.3	**1.9**	8.1×10^{-9}	3.5	1.5

Table 3: **Summary of contrasts, gains and FAC for the OS11 HLC dataset**. Values are integrated over an annular mask of radius 3 to 5 λ/D. The gain is defined by the ratio of contrast after post-processing to the roll combined raw contrast. The Factor Above Classical (FAC) is defined by the ratio of contrast after post-processing with cADI or KLIP to the single roll contrast. The post-processing factors for the no-MUFs and MUFs cases are represented in bold.

Post-Processing Method	Noiseless			Noisy		
	5σ contrast	Gain	FAC	5σ contrast	Gain	FAC
No MUFs						
No sub., single roll minus	4.5×10^{-9}			8.3×10^{-9}		
No sub., single roll plus	4.8×10^{-9}			8.2×10^{-9}		
No sub., roll combined	4.1×10^{-9}			6.0×10^{-9}		
cRDI, single roll	7.2×10^{-10}	6.5		7.0×10^{-9}	1.2	
cRDI, roll combined	5.9×10^{-10}	6.7	1.2	4.5×10^{-9}	1.3	1.1
cADI, roll combined	4.0×10^{-10}	10.3	1.8	5.6×10^{-9}	1.02	0.9
KLIP RDI, roll combined	4.2×10^{-10}	10.9	**1.7**	4.7×10^{-9}	1.4	1.2
With MUFs						
No sub., single roll minus	1.5×10^{-8}			1.6×10^{-8}		
No sub., single roll plus	1.5×10^{-8}			1.8×10^{-8}		
No sub., roll combined	1.3×10^{-8}			1.4×10^{-8}		
cRDI, single roll	1.2×10^{-9}	12.9		8.4×10^{-9}	2.0	
cRDI, roll combined	1.1×10^{-9}	12.1	1.0	5.8×10^{-9}	2.6	1.3
cADI, roll combined	6.0×10^{-10}	22.3	1.9	7.5×10^{-9}	1.9	0.95
KLIP RDI, roll combined	6.1×10^{-10}	24.7	**2.0**	5.7×10^{-9}	2.9	1.5

Table 4: **Summary of contrasts, gains and FAC for the OS9 HLC datasets**. Values are integrated over the annular mask for the region we are the most interested in, which is between 3 and 5 λ/D. The gain is defined by the ratio of contrast after post-processing to the roll combined raw contrast. The Factor Above Classical (FAC) is defined by the ratio of contrast after post-processing with cADI or KLIP to the single roll contrast. The post-processing factors for the no-MUFs and MUFs cases are represented in bold.

Post-Processing Method	Noiseless			Noisy		
	5σ contrast	Gain	FAC	5σ contrast	Gain	FAC
No MUFs						
No sub., single roll minus	1.7×10^{-8}			1.9×10^{-8}		
No sub., single roll plus	1.7×10^{-8}			1.9×10^{-8}		
No sub., roll combined	1.2×10^{-8}			1.3×10^{-8}		
cRDI, single roll	1.7×10^{-9}	10.0		8.8×10^{-9}	2.2	
cRDI, roll combined	1.3×10^{-9}	9.2	0.9	6.2×10^{-9}	2.1	1.0
cADI, roll combined	3.9×10^{-10}	30.7	3.1	8.3×10^{-9}	1.6	0.7
KLIP RDI, roll combined	1.2×10^{-9}	13.7	**1.4**	6.0×10^{-9}	3.0	1.4
With MUFs						
No sub., single roll minus	2.9×10^{-8}			3.0×10^{-8}		
No sub., single roll plus	2.9×10^{-8}			3.1×10^{-8}		
No sub., roll combined	2.0×10^{-8}			2.1×10^{-8}		
cRDI, single roll	2.9×10^{-9}	10.2		1.1×10^{-8}	2.7	
cRDI, roll combined	2.2×10^{-9}	9.2	0.9	8.0×10^{-9}	2.6	1.0
cADI, roll combined	7.4×10^{-10}	27.1	2.7	1.1×10^{-8}	2.0	0.7
KLIP RDI, roll combined	2.0×10^{-9}	14.4	**1.4**	7.7×10^{-9}	3.9	1.4

Table 5: **Summary of contrasts, gains and FAC for the OS11 HLC dataset - TTR5 region**. Values are integrated over an annular mask of radius 6 to 9 λ/D. The gain is defined by the ratio of contrast after post-processing to the roll combined raw contrast. The Factor Above Classical (FAC) is defined by the ratio of contrast after post-processing with cADI or KLIP to the single roll contrast. The post-processing factors for the no-MUFs and MUFs cases are represented in bold.

4 Conclusions

We evaluated the performance of post-processing techniques on OS11 Hybrid Lyot Coronagraph simulated data, which is expected to be the last end-to-end time series for this instrument. Thus, those are the final predicted performance after post-processing of Roman Coronagraph simulated data. The following conclusions are drawn from results compiled in an 3 to $5\lambda/D$ annular mask:

- The factor above classical is equal to 1.9 and 1.7 in the MUF/Noiseless and no MUF/Noiseless case scenarios respectively;

- The performance is better than the design requirement of 10σ flux ratio sensitivity of 5×10^{-8} for every case tested (with and without model uncertainty factor for both noiseless and noisy data);

- In the noisy case, photon noise, rather than residual speckles, is the limiting factor.

- The integrated contrast gain vs. raw contrast between 3 and 5 λ/D from post-processing ranges from ~ 1.3 for the noisy case without model uncertainty factor to ~ 18.8 for the noiseless case with MUF factor;

- ADI performs better in the noiseless case, which is speckle dominated, and RDI performs better in the noisy case, which is shot noise dominated;

- Overall OS11 sensitivities are slightly worse than OS9 sensitivities up to a factor of 3 for the noiseless cases. Changes in the integrated model, including some new error sources and disturbances, likely explain this difference as well as a higher starting dark hole contrast (4×10^{-9} in OS11 vs 1×10^{-9} in OS9)

- Gains and FAC are also significantly smaller for the noiseless case. The noisier LOWFSC correction from the OS11 distribution is likely the cause of the differences between the two distributions.

- Gains are slightly higher for OS11 in the noisy case, it's unclear what may be causing this without further investigation. The OS11 distribution does not have an official "noisy" data release. Instead an example code is provided for users to tailor to their needs. So the comparison of noisy data results from both distributions is likely not an apple-to-apple comparison. Note that the OS11 reference data are photon-counted and it would be interesting to understand whether this choice has a positive impact on the final gains, to better inform the observing strategy.

The following conclusions are drawn from results compiled in an 6 to $9\lambda/D$ annular mask, consistent with TTR5:

- The factor above classical is equal to 1.4 in both the MUF/Noiseless and no MUF/Noiseless case scenarios;

- The performance is better than the design requirement of 10σ flux ratio sensitivity of 5×10^{-8} for every case tested (with and without model uncertainty factor for both noiseless and noisy data);

- In the noisy case, photon noise, rather than residual speckles, is the limiting factor.

- The integrated contrast gain vs. raw contrast between 6 and 9 λ/D from post-processing ranges from ~ 1.6 for the noisy case without model uncertainty factor to ~ 30.7 for the noiseless case with MUF factor;

- ADI performs better in the noiseless case, which is speckle dominated, and RDI performs better in the noisy case, which is shot noise dominated;

- Overall OS11 sensitivities are slightly worse than OS9 sensitivities. Changes in the integrated model, including some new error sources and disturbances, likely explain this difference as well as a higher starting dark hole contrast (4×10^{-9} in OS11 vs 1×10^{-9} in OS9)

- We observe better gains from classical RDI, ADI and KLIP RDI but worse FAC, the classical PSF subtraction performing significantly better on the 6 to $9\lambda/D$ annular mask than on the 3 and $5\lambda/D$ annular mask, which is closer to the star. This points to more stable speckles at large separations, which is to be expected.

5 Acknowledgment

6 References

1. Ygouf et al., "Roman Coronagraph Instrument Post-Processing Report - OS9 HLC Distribution", 2021

2. Nemati, "Photon Counting and Precision Photometry for the Roman Space Telescope Coronagraph", Proc. of SPIE, 2020.

3. Zimmerman et al., "WFIRST Coronagraph Instrument post-processing algorithms for advanced PSF subtraction", 2018.

4. Ygouf et al., "Data processing and algorithm development for the WFIRST-AFTA coronagraph", Proc. of SPIE, 2016.

5. Ygouf et al., "Data Post Processing and Algorithm Development for the WFIRST-AFTA Coronagraph", FY15 final report, Space Telescope Science Institute, 2016.

6. Ygouf et al., "Data Processing and Algorithm Development for the WFIRST-AFTA Coronagraph: Reduction of Noise Free Simulated Images, Analysis and Spectrum Extraction with Reference Star Differential Imaging", Proc. of SPIE, 2015.

7. Ygouf et al., "Data Post-Processing and Algorithm Development for the WFIRST-AFTA Coronagraph", First Progress Report, Space Telescope Science Institute, 2015.

8. Ygouf et al., "AFTA Coronagraphic Technology – Data Post-Processing and Algorithm Development", FY14 final report, Space Telescope Science Institute, 2014.

9. Soummer et al., "Detection and Characterization of Exoplanets and Disks Using Projections on Karhunen-Loève Eigenimages", ApJ, 2012.